Magnetic Resonance in Medicine 63:1716–1722 (2010)

Improved 3-Tesla Cardiac Cine Imaging Using Wideband

Hsu-Lei Lee,[1]* Ajit Shankaranarayanan,[2] Gerald M. Pohost,[3] and Krishna S. Nayak[1,3]

Cine balanced steady-state free precession (SSFP) is the most widely used sequence for assessing cardiac ventricular function at 1.5 T because it provides high signal-to-noise ratio efficiency and strong contrast between myocardium and blood. At 3 T, the use of SSFP is limited by susceptibility-induced off-resonance, resulting in either banding artifacts or the need to use a short-sequence pulse repetition time that limits the readout duration and hence the achievable spatial resolution. In this work, we apply wideband SSFP, a variant of SSFP that uses two alternating pulse repetition times to establish a steady state with wider band spacing in its frequency response and overcome the key limitations of SSFP. Prospectively gated cine two-dimensional imaging with wideband SSFP is evaluated in healthy volunteers and compared to conventional balanced SSFP, using quantitative metrics and qualitative interpretation by experienced clinicians. We demonstrate that by trading off temporal resolution and signal-to-noise ratio efficiency, wideband SSFP mitigates banding artifacts and enables imaging with approximately 30% higher spatial resolution compared to conventional SSFP with the same effective band spacing. Magn Reson Med 63:1716–1722, 2010. © 2010 Wiley-Liss, Inc.

Key words: cardiac ventricular function; balanced SSFP; wideband SSFP; alternating repetition; cine imaging

Cine MRI has been established as a gold standard for the noninvasive assessment of cardiac ventricular function and wall motion (1–3). In clinical practice, the assessment of left ventricular (LV) function includes global measures such as stroke volume, ejection fraction, and cardiac output and regional measures such as wall motion and wall thickening. These assessments require an accurate extraction of the endocardial and epicardial contours. At 1.5 T, balanced steady-state free precession (SSFP) (4,5) is the imaging sequence of choice because it provides (1) strong and uniform contrast between blood and myocardium and between myocardium and epicardial fat, (2) high signal-to-noise ratio (SNR) efficiency, and (3) short acquisition times. Compared to gradient echo approaches, SSFP is less dependent on inflow enhancement, which allows for improved delineation of papillary muscles, trabeculae, and the atrioventricular and semilunar valves (6).

[1]Magnetic Resonance Engineering Laboratory, Ming Hsieh Department of Electrical Engineering, University of Southern California, Los Angeles, California, USA.

[2]Global Applied Science Laboratory, GE Healthcare, Menlo Park, California, USA.

[3]Keck School of Medicine, University of Southern California, Los Angeles, California, USA.

Grant sponsor: National Institutes of Health; Grant number: R21-HL079987; Grant sponsor: American Heart Association; Grant number: #0435249N.

*Correspondence to: Hsu-Lei Lee, Ph.D., University Hospital Freiburg, Department of Radiology, Medical Physics, Breisacher Str. 60a, 79106 Freiburg, Germany. E-mail: hsu-lei.lee@uniklinik-freiburg.de

Received 24 August 2009; revised 20 December 2009; accepted 8 January 2010.

DOI 10.1002/mrm.22384
Published online in Wiley InterScience (www.interscience.wiley.com).

At 3 T, although cardiac imaging can benefit from increased SNR with respect to imaging at 1.5 T (7,8), the use of balanced SSFP for cardiac imaging is fundamentally limited by its sensitivity to off-resonance. Steady-state sequences exhibit signal nulls in their frequency response with periodicity 1/pulse repetition time (TR). The increased susceptibility effects and amplitude of static field inhomogeneities at higher field strengths broaden the off-resonance distribution and demand shorter TR in order to avoid banding artifacts from the signal nulls (9). Schär et al. (10) demonstrated that TR $\leq$3.8 ms was needed to avoid banding artifacts in a group of 13 healthy volunteers. A short TR leads to limited spatial resolution as a direct result of the limited usable readout time, which can affect the accuracy of cardiac function assessment. In clinical settings, the TR could be even more limited for patients with implants, sternal wires, etc. and may require a larger band spacing in order to produce artifact-free images. To achieve adequate spatial resolution without introducing banding artifacts, more general solutions are needed for high-field cardiac MRI.

Alternating TR SSFP methods have been recently developed, which modify the spectral response of SSFP by modulating the repetition times and using specially designed phase-modulation schemes (11). Wideband SSFP is one such alternating TR scheme that uses 0-π phase cycling to widen the central band spacing and relax the TR limitation (12). It allows for a flexible trade-off of the high SNR of 3 T SSFP for an increased bandwidth (up to 2$\times$) and has the ability to suppress banding artifacts in cardiac imaging for a desired spatial resolution. In this work, we apply wideband SSFP to the imaging of LV function at 3 T and demonstrate reduced banding artifact and improved spatial resolution, while retaining the advantageous features of SSFP (speed, contrast, SNR efficiency). We implemented prospectively gated cardiac cine wideband SSFP pulse sequences and performed several tests to examine the reduction of banding artifact, improvement in spatial resolution, and relative SNR efficiency compared to conventional SSFP. Wideband SSFP was able to use a longer readout window than conventional balanced SSFP before banding artifacts became apparent. We demonstrate that wideband SSFP can be used with a TR larger than 5 ms, which can support submillimeter spatial resolution with conventional gradient hardware. Finally, clinical interpretation of complete multislice LV function studies revealed that wideband SSFP increased the number of LV segments that could be assessed and improved overall image quality.

THEORY

Wideband SSFP uses two alternating repetition times (TR and TR_s) and alternating radiofrequency (RF) phase

(0-π) to establish an oscillating steady state with an improved spectral response. This spectral response has null-to-null band spacing of approximately $2/(TR + TR_s)$ (12), which is larger than the band spacing of conventional SSFP (1/TR) when $TR_s < TR$. The signal magnitude on resonance when using wideband SSFP can be expressed as a function of flip angle α, T_1, T_2, and the *a*-factor, defined as TR_s/TR (12):

$$|M_{xy}| = \frac{[(a + \cos\alpha)\frac{T_1}{T_2} + (1 - a\cos\alpha)]\sin\alpha}{(1 - \frac{T_1}{T_2})^2 \sin^2\alpha + \frac{T_1}{T_2}(\sqrt{a} + \frac{1}{\sqrt{a}})^2} \quad [1]$$

The *a*-factor in the multislice LV function studies ranged from 0.53 to 0.73, which gives wideband SSFP an average of 25% increase in band spacing over balanced SSFP with the same imaging TR.

MATERIALS AND METHODS

Experimental Methods

In vivo experiments were performed on a commercial 3-T scanner (Signa Excite HD; GE Healthcare, Waukesha, WI), with gradients supporting a maximum amplitude of 40 mT/m and maximum slew rate of 150 mT/m/ms. The body coil was used for RF transmission and an eight-channel cardiac phased-array coil was used for signal reception. The receiver bandwidth was set to ±125 kHz (4 μs sampling). Localized shimming was performed with the shim volume placed over the left ventricle. A scout sequence with varying frequency offset was used to identify optimal receiving frequency (13). Two-dimensional cine images were obtained with sequential *k*-space segmentation. Electrocardiography gating was used and subjects were instructed to hold their breath at a comfortable exhaled position during each image acquisition. In total, 12 healthy subjects (nine male/three female, age 26–35 years) were scanned during initial testing of the methods and for the experiments described below. Written informed consent was provided before each scan and with an imaging protocol approved by our institutional review board. Data were only collected during TR, and not TR_s. As a result, while keeping the total scan time unchanged, the temporal resolution of wideband SSFP cine data was lower than that of conventional SSFP by a factor of $(1 + a)$. In all studies, image contrast-to-noise ratio (CNR) was calculated as $SNR_{blood} - SNR_{myocardium}$. Signal intensity was measured as the average magnitude over region of interests in myocardium and LV blood pool at both end-diastolic and end-systolic phases (14). Noise was measured as the signal standard deviation outside the body.

Numerical Simulations

Numerical simulations based on Eq. 1 were performed in Matlab to determine blood and myocardium signal intensity as functions of flip angle and *a*-factor. T_1/T_2 values used in simulations were 1100/40 ms for myocardium and 1500/140 ms for blood at 3 T (10). RF excitation profile of a sinc pulse was taken into consideration to more accurately estimate the signal intensity of a real imaging slice. CNR between wideband and balanced SSFP were then calculated from the simulated signal curve.

Evaluation of Off-Resonance Artifacts

In two healthy subjects, balanced SSFP and wideband SSFP CINE loops from a mid short-axis scan plane were obtained with 20 different TR_s and TR combinations (TR ranged from 3.6 to 6.0 ms, and *a*-factor ranged from 0.25 to 1). The scan parameters were field of view = 30 cm, in-plane resolution = 1.2 × 1.2 mm^2 (256 × 256 acquisition matrix), slice thickness = 8 mm, flip angle = 30°. The total scan time was 16 R-R intervals.

Evaluation of the Achievable Spatial Resolution

In two healthy subjects, balanced SSFP and wideband SSFP cine loops were obtained from a three-chamber scan plane, with different spatial resolutions in the readout direction. The imaging TR was set to the minimum according to the desired number of readout points, and the TR_s in wideband SSFP was chosen so that a null-to null band spacing in the frequency response was 300 Hz. Table 1 contains the matrix size, spatial resolution, TR, TR_s, and band spacing of each scan. The remaining scan parameters were field of view = 30 cm, slice thickness = 8 mm, flip angle = 30°, with total scan time of 12 R-R intervals.

Complete LV Function Examinations

In eight subjects, a complete set of short-axis cine loops (eight to 10 slices) was obtained using wideband SSFP and conventional SSFP. Imaging parameters were field of view = 32 × 28.8 cm^2, in-plane resolution = 1.25 × 1.8 mm^2 (256 × 160 acquisition matrix), slice thickness = 8 mm, flip angle = 45°. Imaging TR was set to the minimum according to the desired readout matrix size and ranged from 3.8 to 4.3 ms in different subjects. TR_s in wideband SSFP was chosen so that the null-to-null band spacing was 300 Hz. The total scan time was 10 R-R intervals, with temporal resolution ~30 ms for balanced SSFP and ~50 ms for wideband SSFP. Simulations suggest that with these parameters the null-to-null spacing is 312 Hz for wideband SSFP and 250 Hz for SSFP.

Three physicians experienced in the use of cardiac MRI evaluated the multislice studies in a double-blinded fashion with a two-step approach. At the first step, each physician was then asked to consider each subject separately and select which acquisition provided better image quality, or indicate equivalent quality. The better image series was then assigned the rank 1, and the other was assigned 0. At the second step, the images were graded based on a segment-by-segment basis with the 16-segment model (15). Each of the 16 covered segments (apex was excluded from analysis) was graded on a four-point scale, as follows: 3 = no artifact present, 2 = artifact present but does not adversely affect assessment of wall motion, 1 = artifact present and partially obscures assessment of wall motion, 0 = artifact present and totally obscures assessment of wall motion. A signed

Table 1
Scan Parameters for the In Vivo Evaluation of Spatial Resolution*

Matrix size	192 × 192	256 × 192	320 × 192	384 × 192
In-plane resolution (mm^2)	1.6 × 1.6	1.2 × 1.6	0.9 × 1.6	0.8 × 1.6
TR (ms)	3.4	3.7	3.9	4.2
TR_s (ms)	–	2.9	2.7	2.4
Band spacing of balanced SSFP (Hz)	294	278	256	238
Band spacing of wideband SSFP (Hz)	–	303	303	303
Temporal resolution of balanced SSFP (ms)	54	60	62	68
Temporal resolution of wideband SSFP (ms)	–	106	106	106

*In all cases, the minimum possible TR was used. TR_s in wideband SSFP was chosen such that the band spacing was at least 300 Hz.

rank test was then used to compare the wideband and balanced SSFP image artifact scores across all eight subjects and a total of 128 segments, with the null hypothesis that scores of both sequences have equal median.

RESULTS

Numerical Simulations

Figure 1 contains simulations of balanced SSFP and wideband SSFP blood/myocardium signals as functions of flip angle. All other imaging parameters are the same as in the LV function imaging protocol. The optimum flip angle in terms of CNR was found to be 75° for balanced SSFP and 70° for wideband SSFP with $a = 0.6$. The maximum achievable CNR of wideband SSFP (with a 70° flip angle) is 72% of that of balanced SSFP (with a 75° flip angle). In practice, the in vivo imaging flip angle is limited primarily by RF heating, and a smaller angle has to be used. For flip angles between 30° and 90°, the wideband SSFP CNR is approximately 70% of that of balanced SSFP.

Figure 2 contains numerical simulations of blood/myocardium CNR for the LV function imaging protocol as a function of a-factor. Blood/myocardium CNR is reduced as a-factor decreases. For $a = 0.75$ and 0.5, the CNR of wideband SSFP is estimated to be 84% and 64% of that of conventional balanced SSFP, respectively.

In Vivo Evaluation of Off-Resonance Artifacts

Figure 3 shows LV images (end diastolic frames from CINE loops) acquired with balanced and wideband SSFP with different TR_s and TR values. Dotted and dashed lines represent the contour of equivalent-band spacing in the spectral response. As expected, the banding-related artifacts increase with TR, and the SNR decreases with a-factor. A band spacing >250 Hz can eliminate most severe flow transient artifacts (as the white arrows indicate), which is consistent with literature reports that the off-resonance bandwidth across the human heart on commercial 3-T systems is approximately 260 Hz (7).

Table 2 contains CNR measurements from images with TR = 3.6 ms and 4.0 ms. In the magnitude images, the signal outside of the body has a Rayleigh distribution. Its standard deviation was used as noise magnitude for SNR and CNR calculation. The average CNR of wideband SSFP with $a = 0.75$ and 0.5 was 88% and 71% of that of balanced SSFP, respectively, and is comparable with values predicted by numerical simulation. Images with longer TR were not used for this comparison, because signal measurement was complicated by the presence of

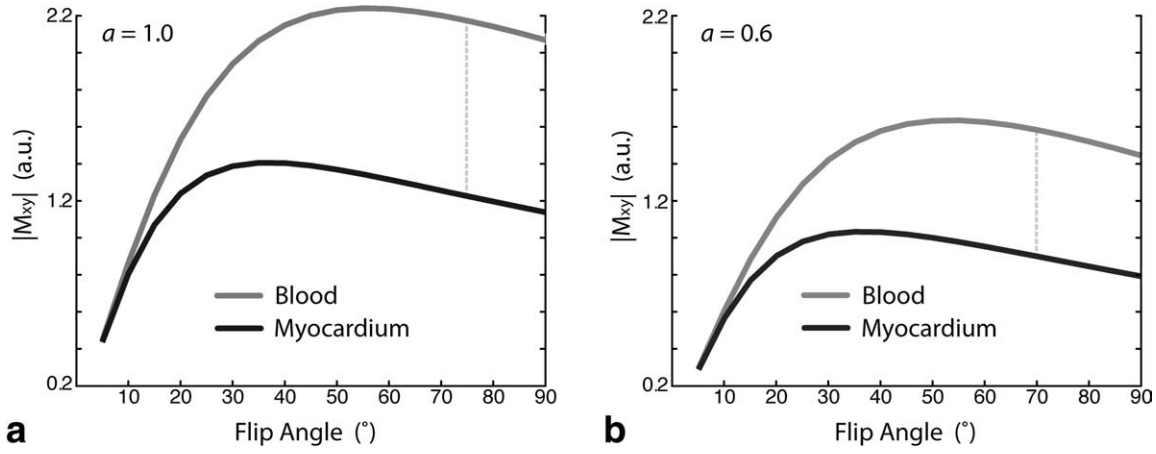

FIG. 1. Numerical simulations of steady-state blood and myocardium signal for **(a)** balanced SSFP and **(b)** wideband SSFP with $a = 0.6$. The flip angles that achieved maximum CNR were 75° for balanced SSFP and 70° for wideband SSFP (gray lines). The simulations are based on $T_1/T_2 = 1100/40$ ms for myocardium and $T_1/T_2 = 1500/140$ ms for blood at 3 T (10). Slice profile effects were taken into consideration.

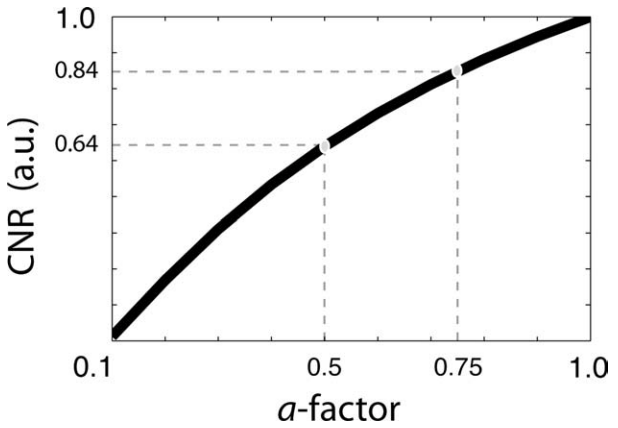

FIG. 2. Blood-myocardium CNR of wideband SSFP as a function of *a*-factor. The CNR increases monotonically with the *a*-factor. Note that $a = 1.0$ is equivalent to conventional balanced SSFP. The simulations were based on a flip angle of 30°.

substantial transient flow artifacts in the balanced SSFP images.

In Vivo Evaluation of the Achievable Spatial Resolution

Figure 4 shows wideband SSFP and conventional balanced SSFP three-chamber images with different spatial resolutions. As the readout matrix was getting larger, the required TR was also longer. At a spatial resolution of 0.8 $\times$ 1.6 mm^2, wideband SSFP still maintained a homogeneous signal across the ROI while artifacts in balanced SSFP increased with TR and obstructed the visualization of LV walls and the valves. Wideband SSFP images avoided these severe artifacts. With reduction in CNR, it provided a consistent image quality when TR was increased.

Complete LV Function Examinations

Figure 5 contains samples of multislice short-axis image sets obtained with wideband SSFP and conventional balanced SSFP. Both sequences showed high contrast between blood and myocardium. The average blood-myocardium CNR was 40 for balanced SSFP and 32.3 for wideband SSFP.

The average image quality ranks for each sequence and each reviewer are listed in Table 3. Average rank shows about 70% of the time, wideband SSFP produces an image that is preferable to the reviewers. A histogram depicting the difference of wideband and balanced SSFP myocardial segment scores is shown in Fig. 6. Both sequences have an average score between "no artifact present" and "artifact present but does not adversely affect assessment of wall motion." The signed rank test revealed that for all three reviewers, wideband SSFP images had higher scores than balanced SSFP ($P < 0.05$) over a total of 128 LV segments, indicating a reduction in artifacts with wideband SSFP that improves wall motion assessment.

DISCUSSION

We observe that an imaging sequence with band spacing <250 Hz can easily suffer from substantial off-resonance

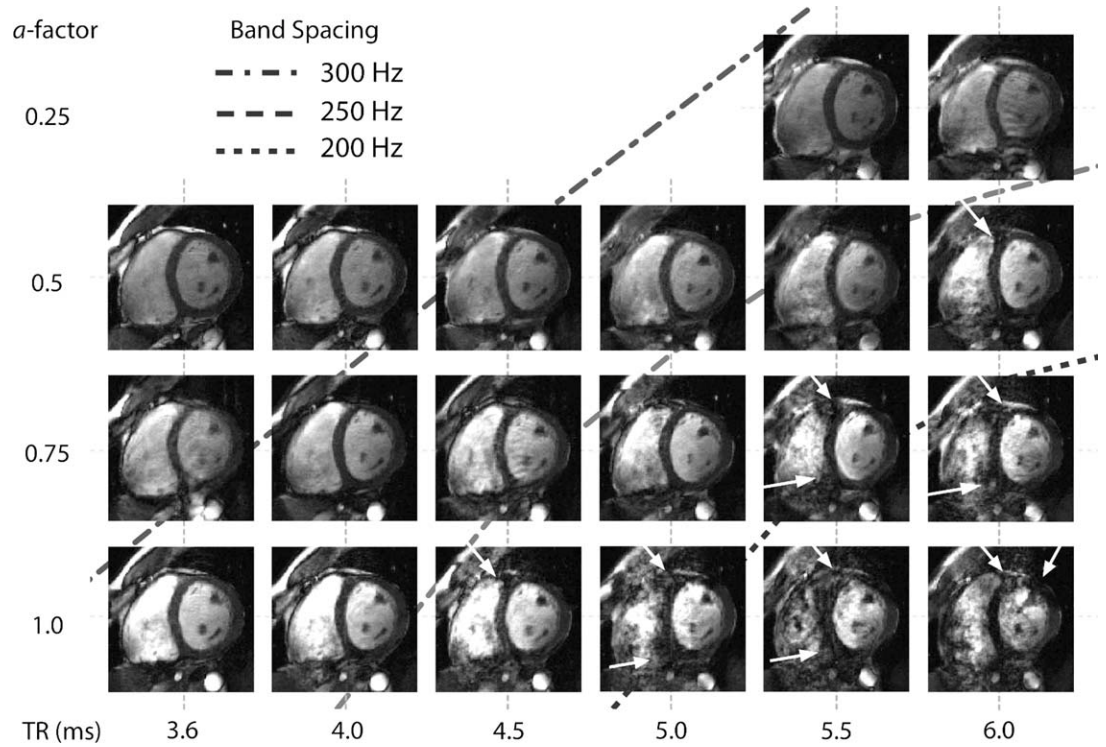

FIG. 3. Comparison of image artifacts with different TR_s/TR combinations. Balanced and wideband SSFP end-diastole frames from short-axis cine images were obtained with different TR_s/TR. Dashed lines and background colors represent band spacing range for the images. White arrows indicate off-resonance artifacts that obstruct the cardiac assessment. Each column represents a fixed imaging TR. The bottom row represents balanced SSFP (TR_s/TR = 1.0). TR_s shortens when moving to the left and therefore widens the band-spacing in the frequency spectrum.

Table 2
Measured Blood-Myocardium CNR for Balanced SSFP and Wideband SSFP*

TR_s/TR ratio	1.0	0.75	0.5
CNR (TR = 3.6 ms)	51.5	43.3	36.7
CNR (TR = 4.0 ms)	59.5	54.5	42.0
Relative CNR	100%	88%	71%

*CNR values of wideband SSFP drops with *a*-factor.

artifact across the heart at 3 T, which is consistent with the literature reports that the off-resonance across left ventricle at 3 T is approximately 260 Hz (7) and can be even larger for the whole heart. Thus, in order to ensure the accurate depiction of myocardial contours, a band spacing $\geq$300 Hz is preferred. In conventional balanced SSFP, this means a TR $\leq$3.4 ms, whereas by shortening TR_s in wideband SSFP, the imaging TR can be extended to up to more than 4.2 ms, and we have demonstrated this increased TR in vivo. Since a longer TR is allowed, spatial resolution can be improved with wideband SSFP while providing reasonable SNR and CNR. As shown in Fig. 4, image quality is preserved by modifying TR_s to maintain sufficient band spacing while extending the readout window for higher spatial resolution. A submillimeter three-chamber image was achieved by wideband SSFP without introducing severe off-resonance artifact. Multislice wideband SSFP images also showed reduced artifacts for a fixed scan parameter set (see Fig. 5), which can provide more reliable assessment to LV function and help to improve the diagnostic quality of cardiac function examinations at 3 T.

In the single-slice scans we performed, $a = 0.75$ provided a CNR that was 88% of balanced SSFP, and $a = 0.5$ provided a CNR that was 71% of balanced SSFP. The amount of reduction was less than theory predicted. There are two possible sources for the underestimation of blood signal. First, magnetizations can generate fluctuating signals before they are fully stabilized. The estimation was based on steady-state signal equations. However, ventricular blood is in fact a pulsatile flow, and it is often in transient state during image acquisition. The image SNR then becomes a complex mixture of multiple transient states that are partial T_2-weighting and deviate from the predicted value. This blood inflow may also contribute to the increase in CNR when imaging TR is longer. The second source is the amplitude of RF field variation in the region of interest (16). In some areas, the spins may not experience a 30° excitation as we prescribed. The variance in flip angles changes the resulted signal intensity and contrast in a nonlinear fashion with respect to both flip angles and *a*-factor.

Another consideration is the fact that RF heating is increased in wideband SSFP sequences. In order to maintain SAR within the safety limits during a steady-

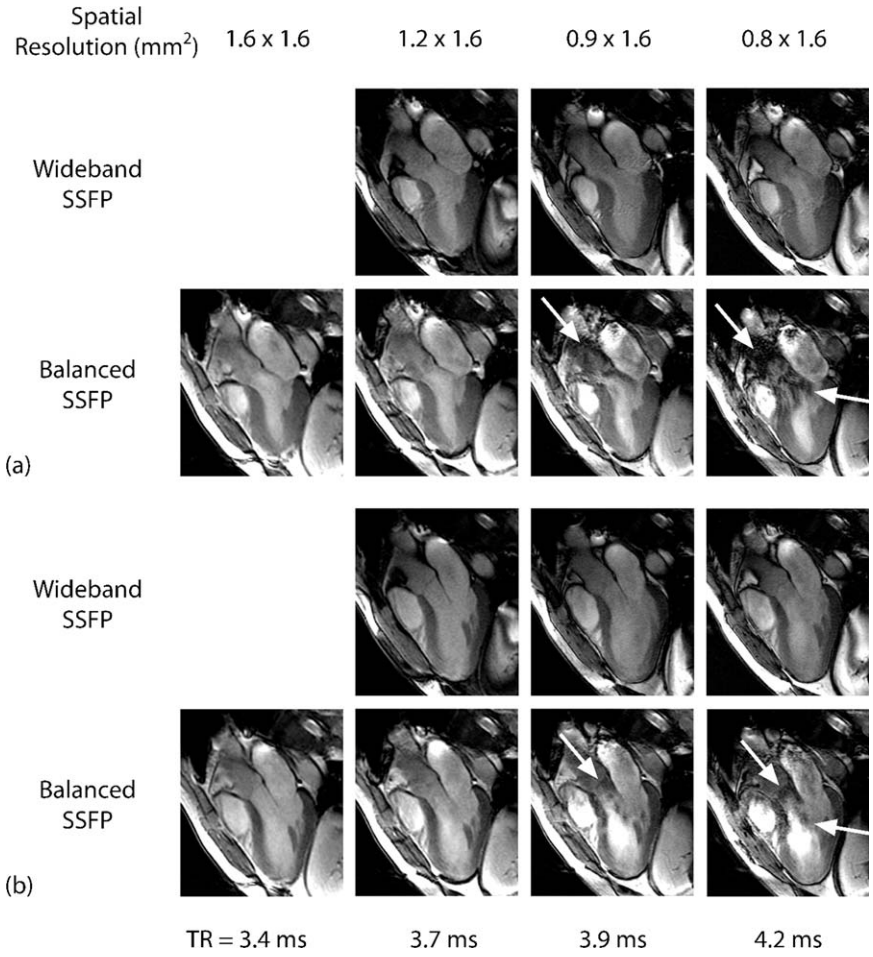

FIG. 4. Balanced and wideband SSFP images from three-chamber cine images with different spatial resolutions. Images are selected from **(a)** end-systole, and **(b)** mid-diastole. White arrows indicate off-resonance artifacts that obstruct the cardiac assessment. Scan parameters: 30° flip angle, 12 R-R breath-hold (see Table 1).

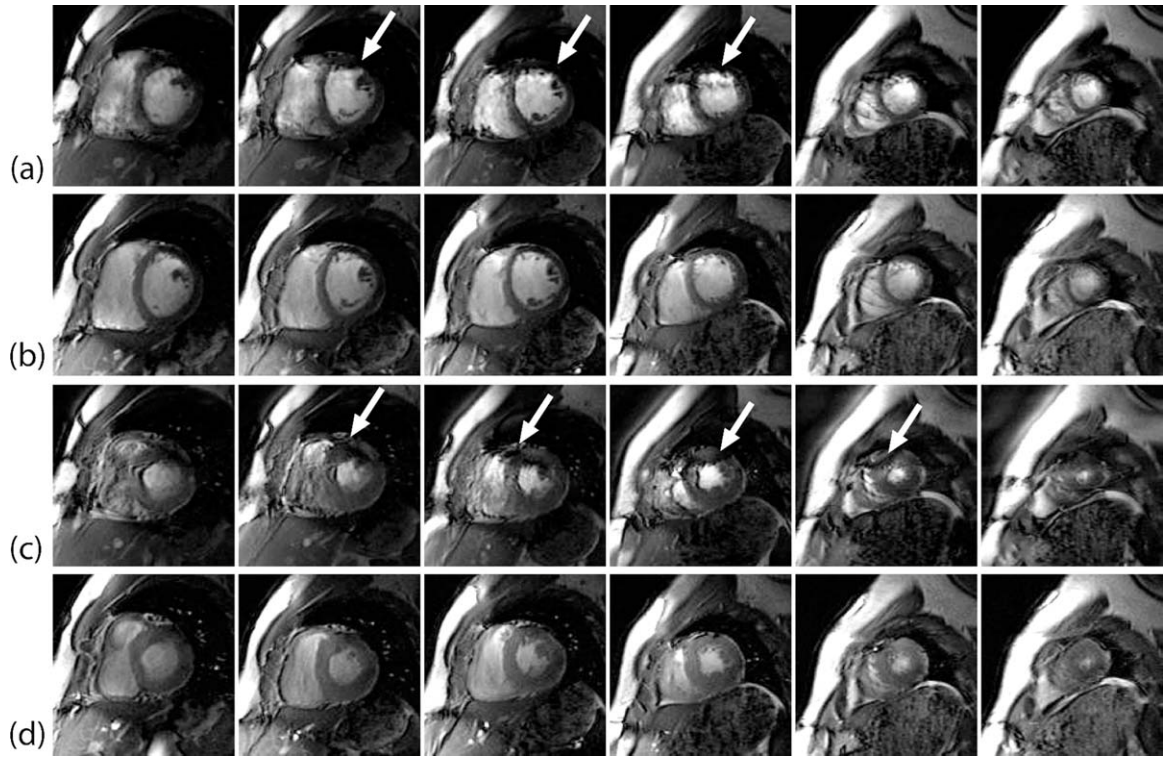

FIG. 5. Multislice short axis cine LV function data acquired with balanced and wideband SSFP in a representative volunteer at 3 T. **a:** Mid-diastole, balanced SSFP; **(b)** mid-diastole, wideband SSFP; **(c)** end-systole, balanced SSFP; **(d)** end-systole, wideband SSFP. White arrows indicate off-resonance artifacts that obstruct the cardiac assessment. Scan parameters: $TR_s/TR = 2.6/4.0$ ms, 30° flip angle, 12 R-R breath-hold per slice.

state scan, the flip angle often has to be reduced, which leads to suboptimal SNR. A flip angle of 45° was used in the multislice LV function imaging conducted in this study. As depicted in Fig. 1, there is no significant change in blood/myocardium CNR for flip angles between 45° and 90°, so the CNR was not substantially affected by the lowered flip angle. However, because of the additional TR_s in wideband SSFP sequences, the number of RF pulses needed to obtain a complete cine series is doubled compared to conventional balanced SSFP (when the same temporal resolution is desired). Depending on the scan condition, the flip angle of wideband SSFP might have to be further reduced. Possible solutions to reduce SAR include implementing variable rate selective excitation (17) excitation pulses and parallel transmission techniques (18), which we did not attempt in this study.

During all the scans in this study, the wideband SSFP has a lower temporal resolution compared to balanced SSFP, while spatial resolution and total breath-hold time were kept the same. This can be compensated for by using parallel imaging without increasing total scan time, when autocalibration signals are acquired during the currently unused short TR_s (19). The TR_s signal can

Table 3
Image Quality Rank of Multislice Cine Imaging*

	Wideband SSFP	Balanced SSFP
Reviewer 1	0.81	0.19
Reviewer 2	0.63	0.38
Reviewer 3	0.69	0.31
Average	0.71	0.29

*Grades were averaged from all subjects.

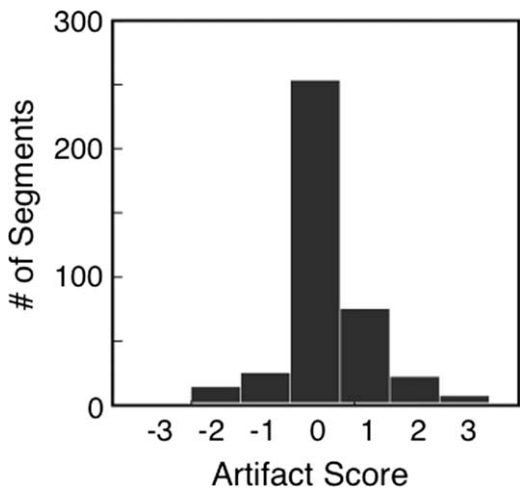

FIG. 6. Distribution of artifact score differences (wideband minus conventional) from all myocardial segments and all reviewers. The scale was 3, no artifact present; 2, artifact present but does not adversely affect assessment of wall motion; 1, artifact present, partially obscures assessment of wall motion; 0, artifact present and totally obscures assessment of wall motion. A signed rank test was applied and determined that wideband SSFP scores have a higher median than balanced SSFP scores, with $P < 0.05$.

also be used for self-navigation, therefore eliminating the need for breath holds during cardiac scans (20).

CONCLUSIONS

We have demonstrated improved cardiac ventricular function imaging at 3 T, using a cine wideband SSFP pulse sequence. By trading off temporal resolution and SNR efficiency, wideband SSFP is able to reduce off-resonance artifact and provide higher and more consistent image quality for cardiac function assessment compared to conventional balanced SSFP of the same spatial resolution. We achieved 0.8×1.6 mm^2 in-plane resolution in single-slice three-chamber imaging and 1.25×1.8 mm^2 in-plane resolution in multislice short-axis LV function imaging, without major artifact. Compared to balanced SSFP, wideband SSFP images received better average scores for overall image quality and local artifact level, as assessed by three independent reviewers. The ability to increase readout duration also makes it possible to acquire high-resolution images or implement time-efficient acquisition schemes (21), which may be used to shorten the length of breath holds or to perform free-breathing real-time imaging. Our preliminary results demonstrate the feasibility and improved image quality of wideband SSFP for cardiac function imaging at 3 T.

ACKNOWLEDGMENTS

Supported by the Zumberge Foundation and GE Healthcare. H.-L. Lee has received support from a USC Viterbi School of Engineering Graduate Fellowship and a USC Women in Science and Engineering Merit Fellowship.

REFERENCES

1. Seminelka RC, Tomei E, Wagner S, Mayo J, Kondo C, Suzuki J, Caputo GR, Higgins CB. Normal left ventricular dimensions and function: interstudy reproducibility of measurements with cine MR imaging. Radiology 1990;174:763–768.
2. Debatin JF, Nadel SN, Paolini JF, Sostman HD, Coleman RE, Evans AJ, Beam C, Spritzer CE, Bashore TM. Cardiac ejection fraction: phantom study comparing cine MR imaging, radionuclide blood pool imaging and ventriculography. J Magn Reson Imaging 1992;2: 135–142.
3. Higgins CB. Which standard has the gold? J Am Coll Cardiol 1992; 19:1608–1609.
4. Oppelt A, Graumann R, Barfuss H, Fischer H, Hartl W, Shajor W. FISP: a new fast MRI sequence. Electromedica 1986;54:15–18.
5. Zur Y, Stokar S, Bendel P. An analysis of fast imaging sequences with steady-state transverse magnetization refocusing. Magn Reson Med 1988;6:175–193.
6. Moon JCC, Lorenz CH, Francis JM, Smith GC, Pennell DJ. Breath-hold FLASH and FISP cardiovascular MR imaging: left ventricular volume differences and reproducibility. Radiology 2002;223:789–797.
7. Noeske R, Siefert F, Rhein KH, Rinneberg H. Human cardiac imaging at 3 T using phased-array coils. Magn Reson Med 2000;44:978–982.
8. Stuber M, Botnar RM, Fischer SE, Lamerichs R, Smink J, Harvey P, Manning WJ. Preliminary report on in vivo coronary MRA at 3 tesla in humans. Magn Reson Med 2002;48:425–429.
9. Duerk JL, Lewin JS, Wendt M, Petersilge C. Remember true FISP? a high SNR, near 1-second imaging method for t2 -like contrast in interventional MRI at 2 T. J Magn Reson Imaging 1998;8:203–208.
10. Schär M, Kozerke S, Fischer SE, Boesiger P. Cardiac SSFP imaging at 3 tesla. Magn Reson Med 2004;51:799–806.
11. Leupold J, Hennig J, Scheffliger K. Alternating repetition time balanced steady state free precession. Magn Reson Med 2006;55:557–565.
12. Nayak KS, Lee HL, Hargreaves BA, Hu BS. Wideband SSFP: alternating repetition time balanced steady state free precession with increased band spacing. Magn Reson Med 2007;58:931–938.
13. Deshpande VS, Shea SM, Li D. Artifact reduction in true-FISP imaging of the coronary arteries by adjusting imaging frequency. Magn Reson Med 2003;49:803–809.
14. Wintersperger BJ, Bauner K, Reeder SB, Friedrich D, Dietrich O, Sprung KC, Picciolo M, Nikolaou K, Reiser MF, Schoenberg SO. Cardiac steady-state free precession cine magnetic resonance imaging at 3.0 tesla: impact of parallel imaging acceleration on volumetric accuracy and signal parameters. Invest Radiol 2006;41:141–147.
15. Henry WL, DeMaria A, Gramiak R, King DL, Kisslo JA, Popp RL, Sahn DJ, Schiller NB, Tajik A, Teichholz LE, Weyman AE. Report of the American Society of Echocardiography Committee on Nomenclature and Standards in Two-Dimensional Echocardiography. Circulation 1980;62:212–217.
16. Sung K, Nayak KS. Measurement and characterization of RF non-uniformity over the heart at 3T using body coil transmission. J Magn Reson Imaging 2008;27:643–648.
17. Conolly SM, Nishimura DG, Macovski A, Glover G. Variable-rate selective excitation. J Magn Reson 1988;78:440–458.
18. Zhu Y. RF power reduction with parallel excitation. In: Proceedings of the 12th Annual Meeting of the ISMRM, Honolulu, 2004. p 331.
19. Lee HL, Shankaranarayanan A, Pohost GM, Nayak KS. Auto-calibrated parallel imaging using the unused echo in alternating TR SSFP. In: Proceedings of the 17th Annual Meeting of the ISMRM, Kyoto, 2009. p 768.
20. Lee HL, Shankaranarayanan A, Nayak KS. Retrospective self-navigated cine imaging using the unused echo in alternating TR SSFP. In: Proceedings of the 17th Annual Meeting of the ISMRM, Honolulu, 2009. p 4643.
21. Lee HL, Pohost GM, Nayak KS. Gated and real-time wideband SSFP cardiac imaging at 3T. In: Proceedings of the 14th Annual Meeting of ISMRM, Seattle, 2006. p 143.